Supporting information for

Eliminating Trade-Offs Between Optical Scattering and Mechanical Durability in Aerogel as Outdoor Passive Cooling Metamaterials

Chenyang Cai*[1], Yi Chen[1], Chunxiang Ding[1], Zechang Wei[2], and Xuan Wang*[3]

1 Co-Innovation Center of Efficient Processing and Utilization of Forest Resource, School of Materials Science and Engineering, Nanjing Forestry University, Nanjing, Jiangsu, 210037, China

2 College of Chemistry and Materials Engineering, Zhejiang A & F University, Hangzhou 311300, Zhejiang, China

3 Department of Mechanical Engineering, University of North Texas, Denton, Texas 76203, United States

E-mail: ccy@njfu.edu.cn; XuanWang@my.unt.edu

Supplementary Discussion

1. Experimental section

2. Morphology structure of cellulose nanocrystal and cellulose nanofiber

3. Chemical structure of as prepared nanocellulose composite aerogel

4. Reaction process and resulting chemical structure of NCA

5. Morphology structure of nanocellulose composite aerogel

6. Thermal insulation performance of NCA and commercial plastic foams.

7. Calculation of solar reflection and infrared emissivity

8. Finite Element Simulations

9. Cooling energy saving simulation

10. Recycling process of NCA

11. COMSOL stimulation

Experimental Section

Materials

Microcrystalline cellulose (MCC) with an average particle size of 50 μm was kindly provided by Shanhe Pharmaceutical Excipients Co. Ltd., Anhui, China. Cellulose nanofiber was purchased from Zhongshan Nanofiber New Materials Co., Ltd. Ammonium hydroxide and sulfuric acid were bought from Sigma-Aldrich. Methyltrimethoxysilane (MTMS, 98%) was purchased from Innochem. Cellulose nanocrystal (CNC) as raw materials were isolated according to previous work[1]. Deionized water (DI water) was used throughout the experiment. All chemicals were directly used without any other treatment.

Preparation of nanocellulose aerogel (NCA)

Nanocellulose aerogel (NCA) were constructed *via* pre-crosslinking assembly and unidirectional freeze casting technology. First, 30 mL CNC suspensions (8 mg/mL) were added to a 100 mL beaker to get well-dispersed breaks under vigorous stirring for 3 h. After that, 10 g CNF suspensions (2.5 wt%) were added and stirred for 6 h. After that, a drop of NH_4OH (as a catalyst) was added dropwise to the solution for 6 h under vigorous stirring to obtain a homogeneous binary sol. Then, obtained suspensions were poured into a self-made mold to undergo unidirectionally frozen. Finally, they were freeze-dried to obtain the NCA, denoted as NCA1. The NCA2 and NCA3 were prepared by using same method with different CNF loadings: NCA2 (CNF 20 g), NCA 3 (CNF 30g). Meanwhile, the pure CNC aerogel and silane crosslinked CNC aerogel

(C-CNC) were also prepared.

Characterization

The morphology of CNC and CNF were observed by using a transmission electron microscope (JEM-1400, Japan) with an accelerating voltage of 80 kV. Dynamic rheological analyses (DRAs) of suspensions were performed by using a HAAKE RheoStress 600 (Thermo Fisher Scientific Inc. USA). The tests were examined in a frequency-sweep mode with the frequency from 100 to 0.1 Hz in the linear viscoelastic range. The chemical structure of aerogels was evaluated by using Fourier transform infrared spectroscopy (FT-IR, VERTEX 80 V, Bruker, USA) and Axis Ultra DLD spectrometer (Kratos Co., UK). The morphology of nanocellulose aerogel was analyzed on environmental scanning electron microscope (Quanta 200, FEI) at the voltage of 5 kV. Before the observation, the NCA was coated with gold. The compressive tests were performed by using a universal machine (SANS CMT4202, China) equipped with a 50N loading cell. The NCA was compressed with the speed of 5mm/min to 70% of its original thickness. The thermal conductivity was measured on a Hot Disk instrument (TPS2500S, Sweden) with the transient-plane source method. The infrared images of the aerogels were recorded by using an infrared camera (FOTRIC, 250, China). Water contact angle of NCA was tested by using DSA25E ADVANCE machine (KRÜSS, Germany), and 4 μL water droplet was used. The solar reflectance of NCA (0.3-2.5 μm) was measured using an UV–visible–near-infrared spectrophotometer (UV 3600, Shimadzu) equipped with an integrating sphere model (ISR-3100). A Fourier transform

infrared spectrometer (Bruker, INVENIO R) equipped with a gold integrating sphere (Bruker, A562) was also used to measure the IR absorbance (2.5-25 μm).

Outdoor test

The radiative cooling performance of NCA was tested at the Nanjing Forestry university (China). In the self-made thermal box, a bulk of cooling sample (NCA) with a size of 7 cm × 7 cm was used. The thermocouples are used to detect the real-time temperature change of the NCA and the ambient air near the experimental set-up. With the help of the feedback-controlled heating system, the aerogel cooler temperature was maintained at the ambient temperature to minimize the conductive and convective heat loss induced from the surrounding environment. The power provided by the feedback-controlled heat accurately measures the real-time cooling power

Finite Element Simulations:

The finite element simulation is carried out using commercial code ANSYS 2020R2. The CPS4R, a 4-node bilinear plane stress quadrilateral element is used to mesh the NCA model. We strictly maintaining micro structure the same height (21.875 length unit), the same length (35 length unit), and same width (35 length unit) of the entire model with the NCA. The mathematic description of the curved shape is a sinusoidal function, but it adopts a straight-line shape at the contact region between layers. Then an initial separation (0.5 length unit) between the curved layers is introduced in the

NCA structure model for defining the contact between surfaces. Such a contact is modeled by using hard contact as the normal behavior and frictionless resistance as the tangential behavior. Displacement loading is applied as shown in Figure S14. The elastic properties are set as the following - Young's Modulus: 10 GPa, Poisson's ratio: 0.3.

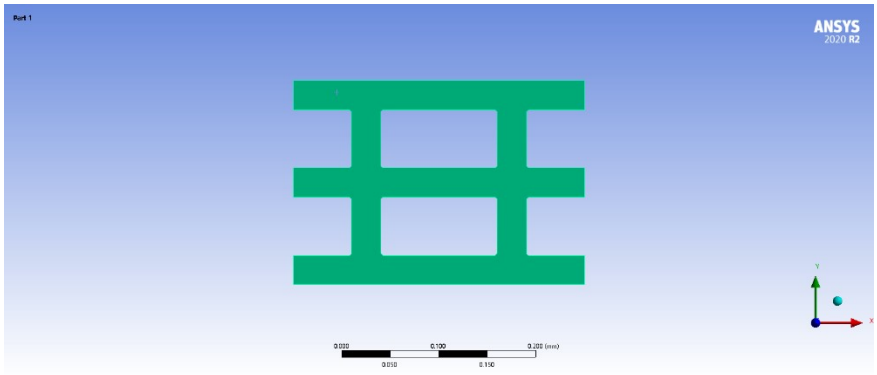

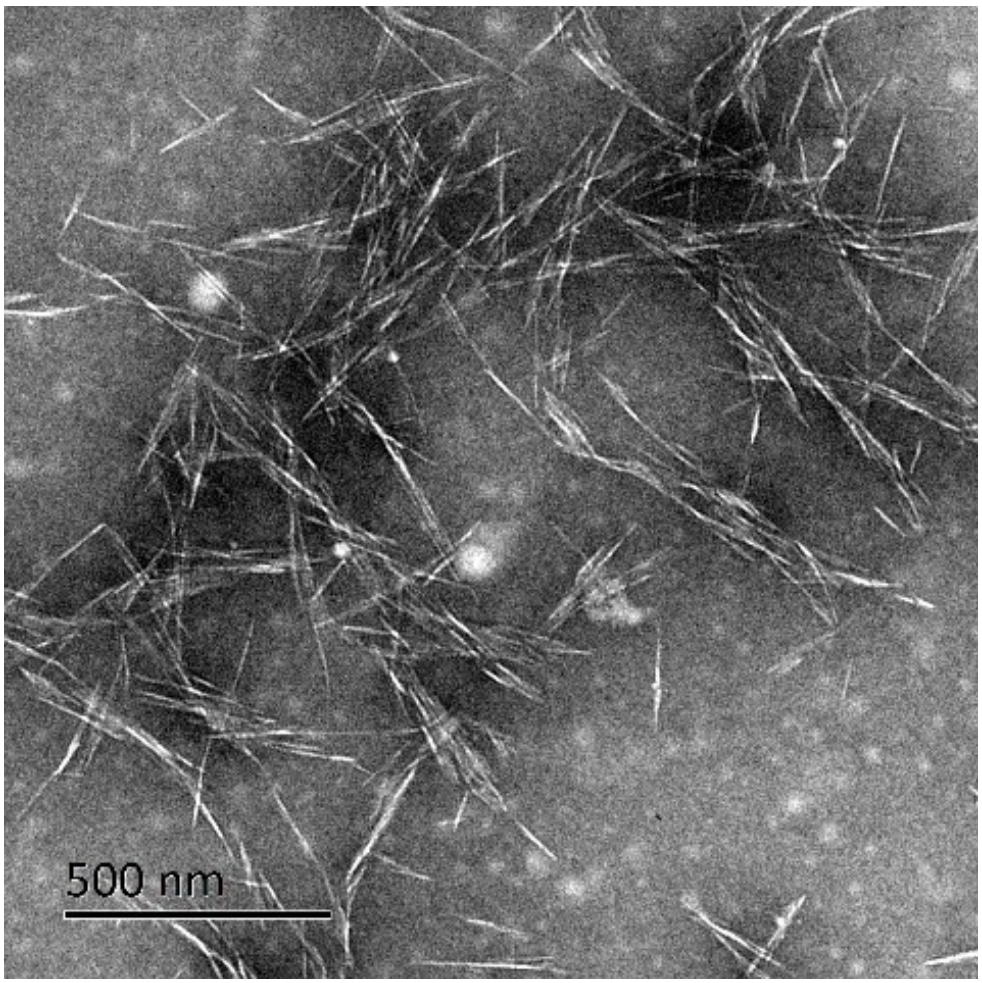

Figure S1 TEM image of cellulose nanocrystal (CNC)

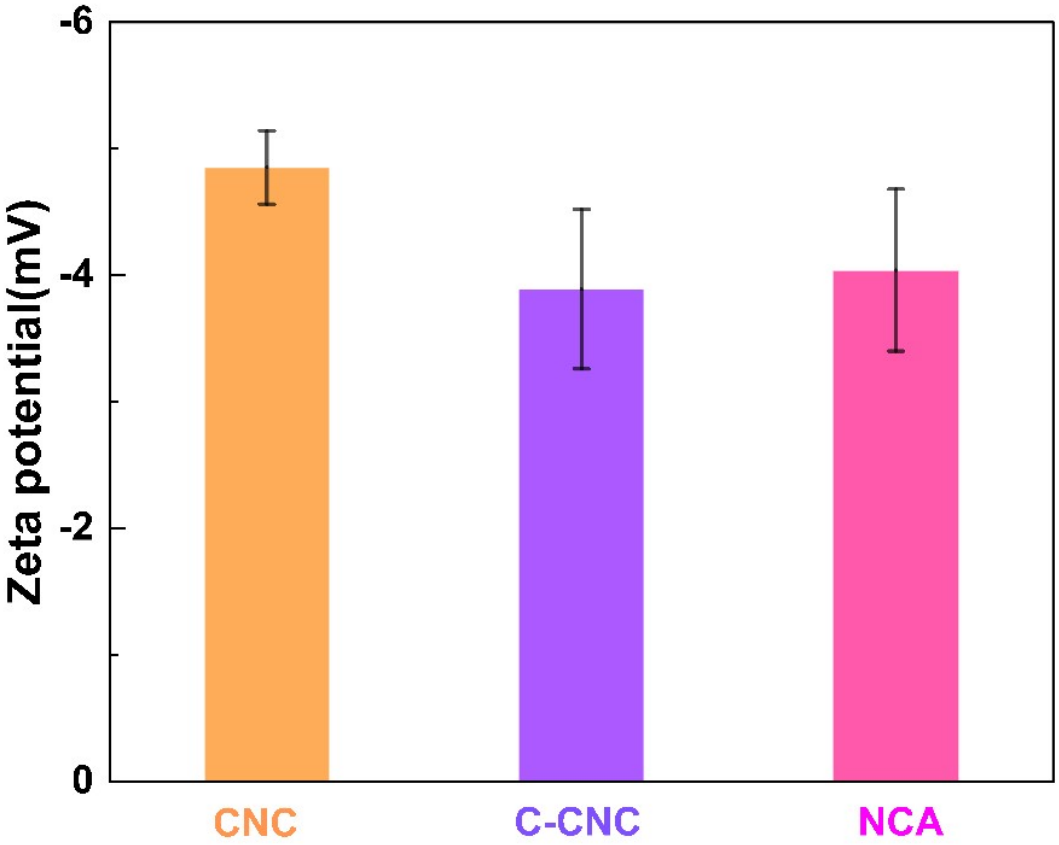

Figure S2 Zeta potential of CNC, C-CNC and CNC-C-CNF (NCA)

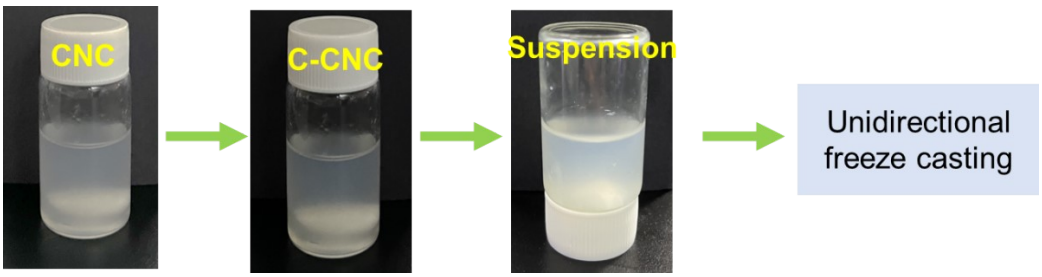

Figure S3 Construction process of crosslinked CNC aerogel

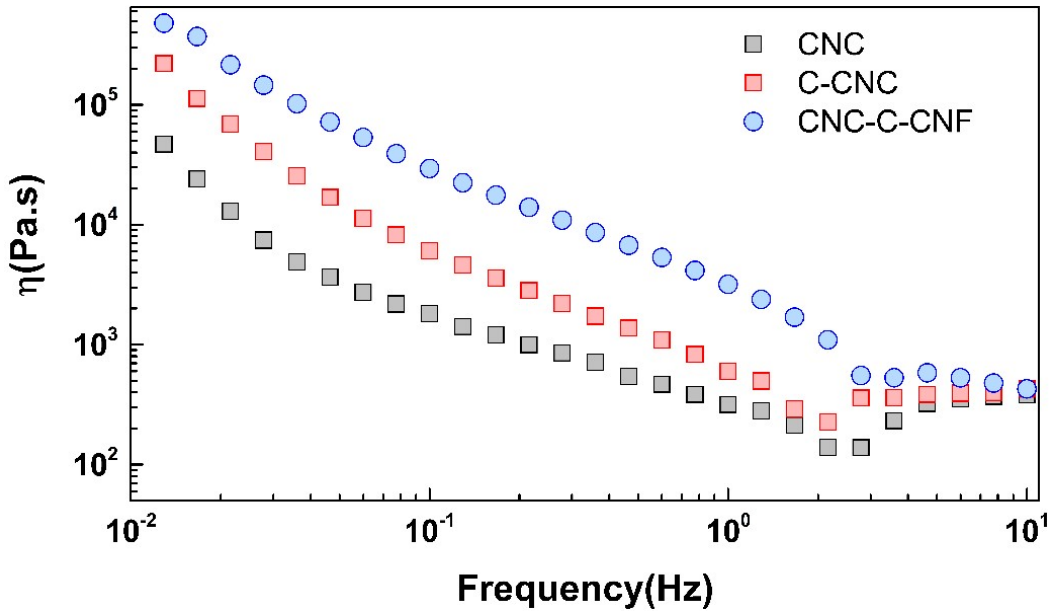

Figure S4 Viscosity of CNC, C-CNC and CNC-C-CNF (NCA) from 10^{-2} to 10 Hz

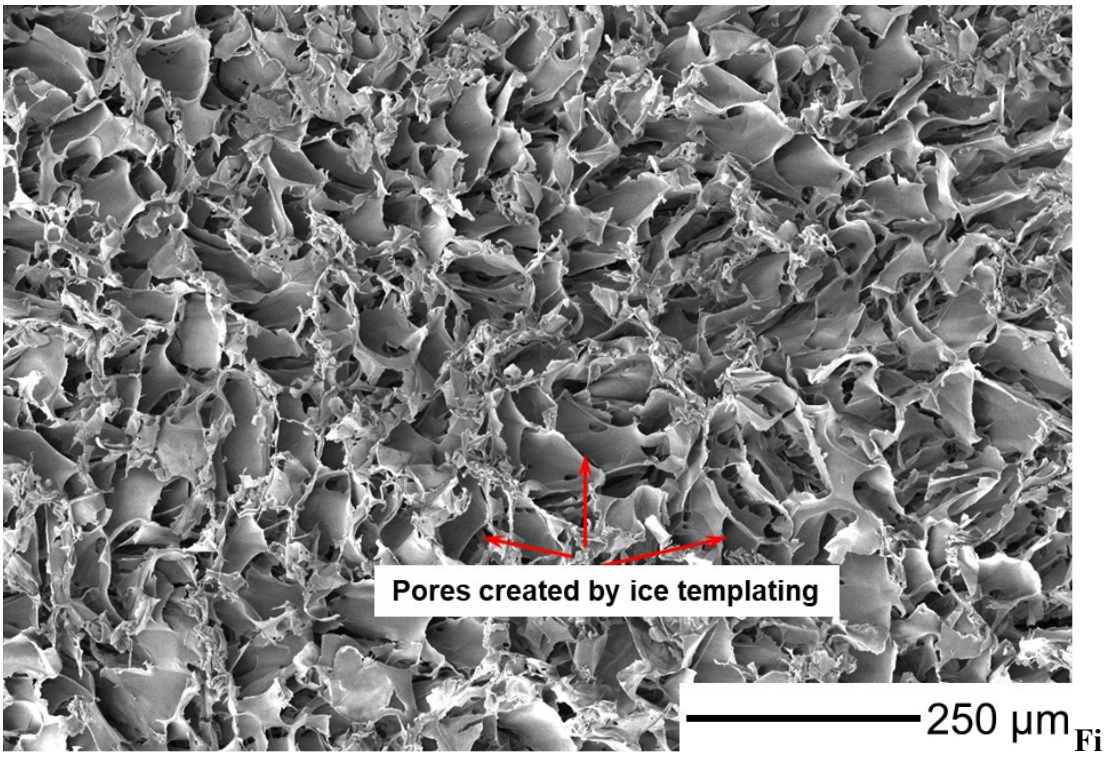

gure S5 Morphology structure of pure CNC aerogel at scale bar of 250 µm: showing irregular pores

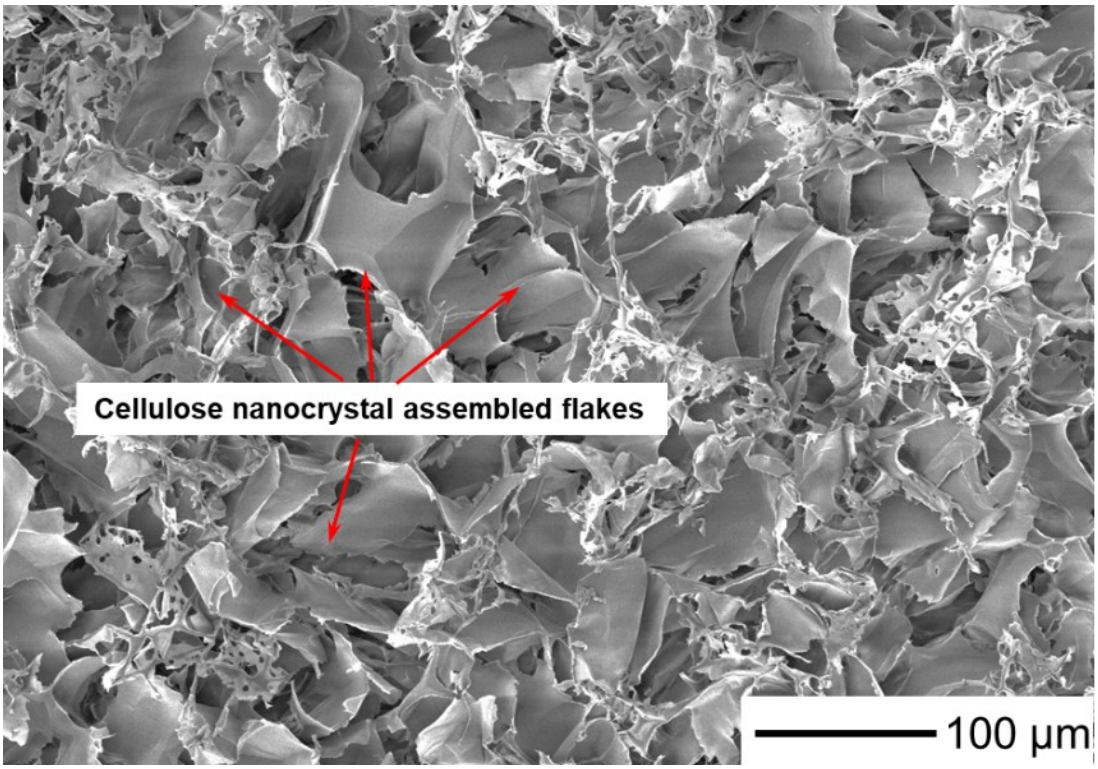

Figure S6 Morphology structure of pure CNC aerogel at scale bar of 100 µm: showing irregular flakes created by cellulose nanocrystal induced by ice templating

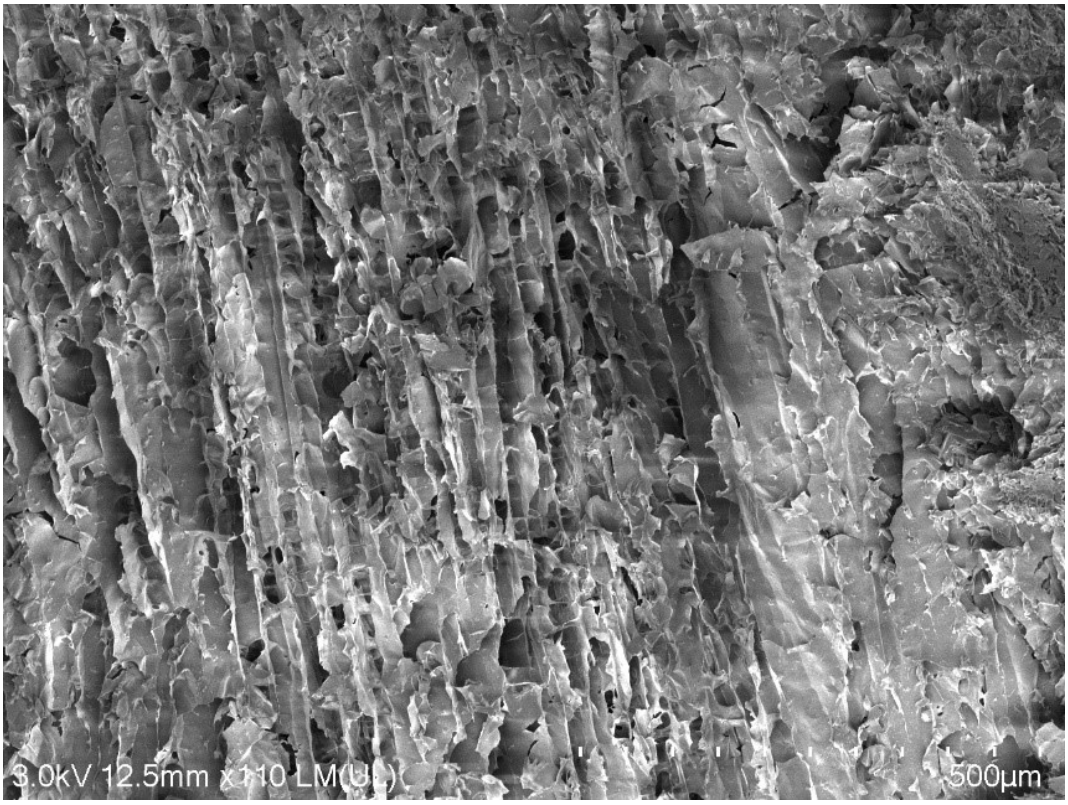

Figure S7 Morphology structure of pure CNC aerogel at scale bar of 500 µm: side view

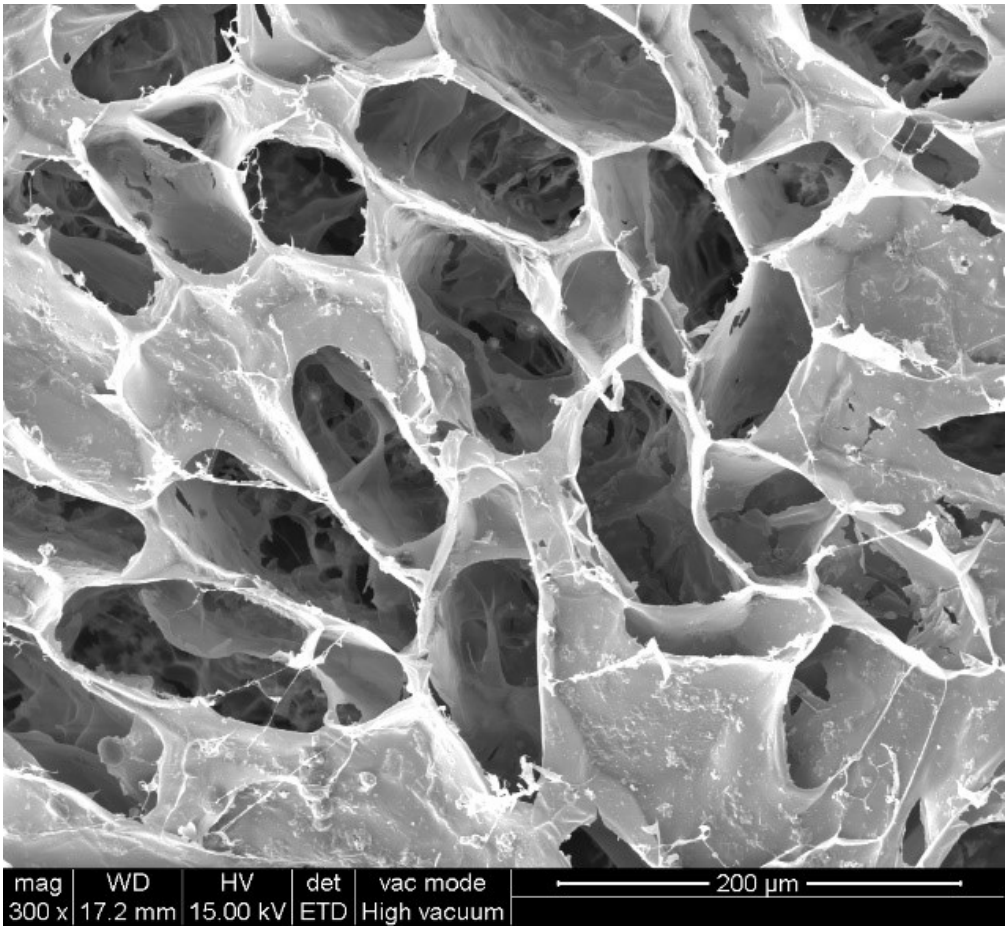

Figure S8 Morphology structure of NCA 1 aerogel: (Left: top view) and (Right: side view)

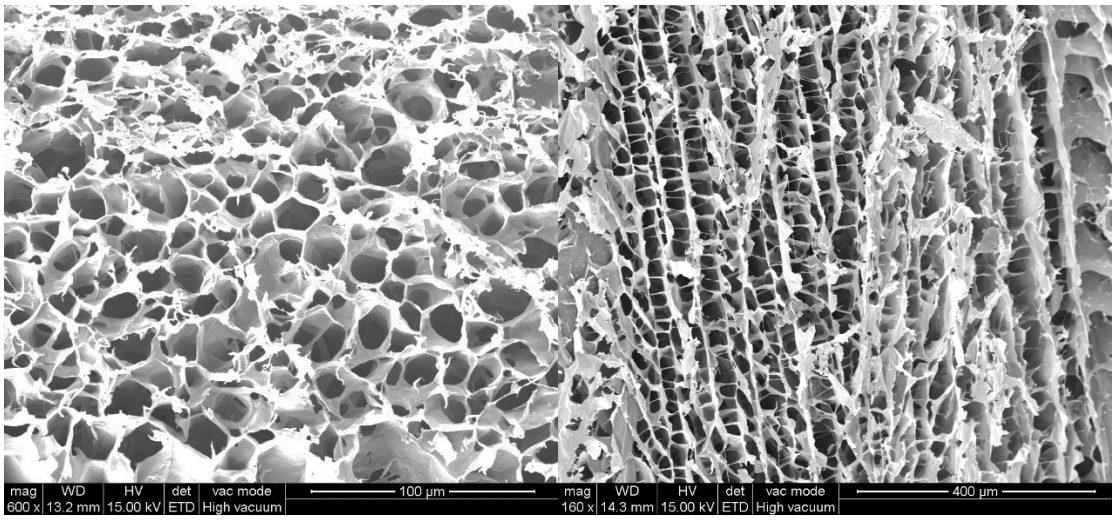

Figure S9 Morphology structure of NCA 2 aerogel: (Left: top view) and (Right: side view)

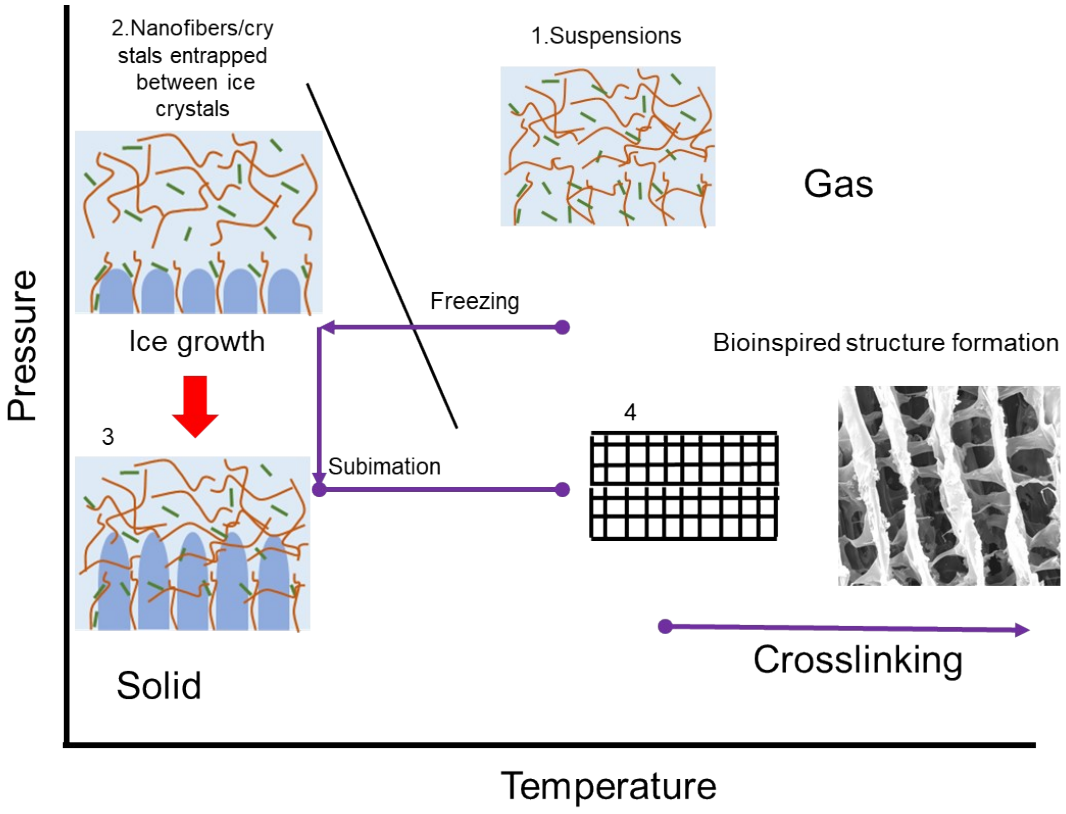

Figure S10 Proposed mechanism of structure formation by using unidirectional technology

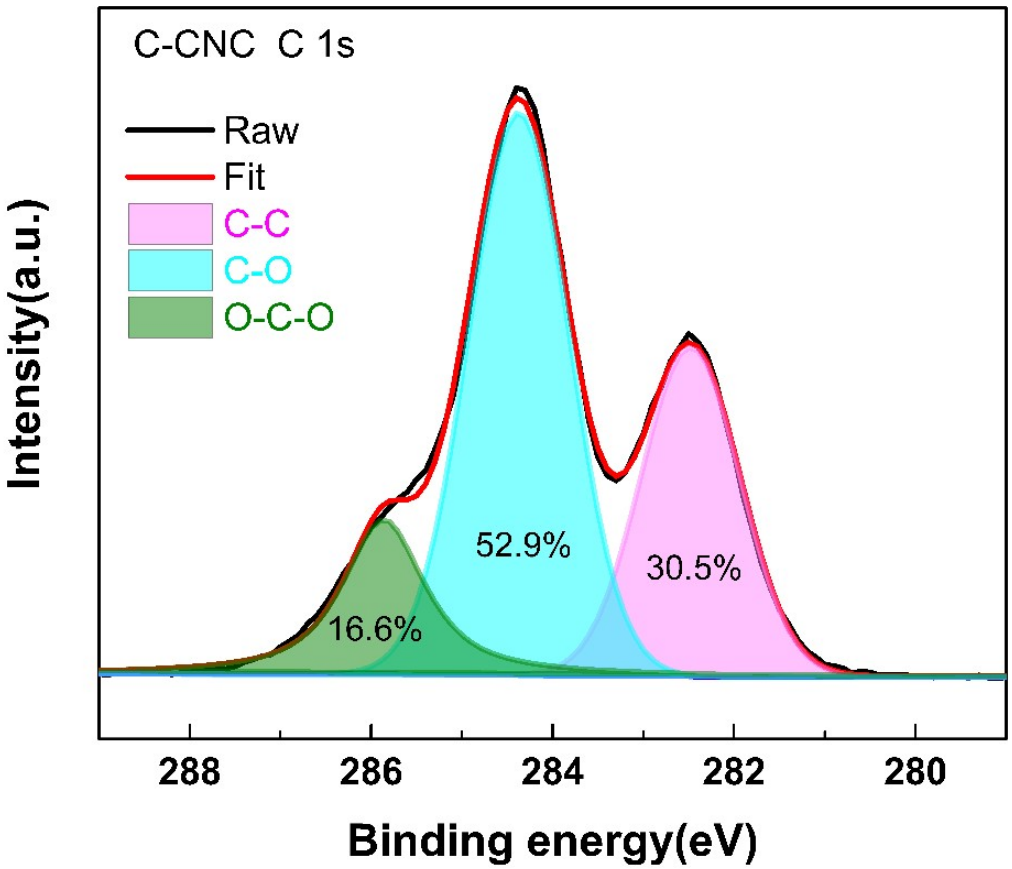

Figure S11 C 1s curve of C-CNC aerogel

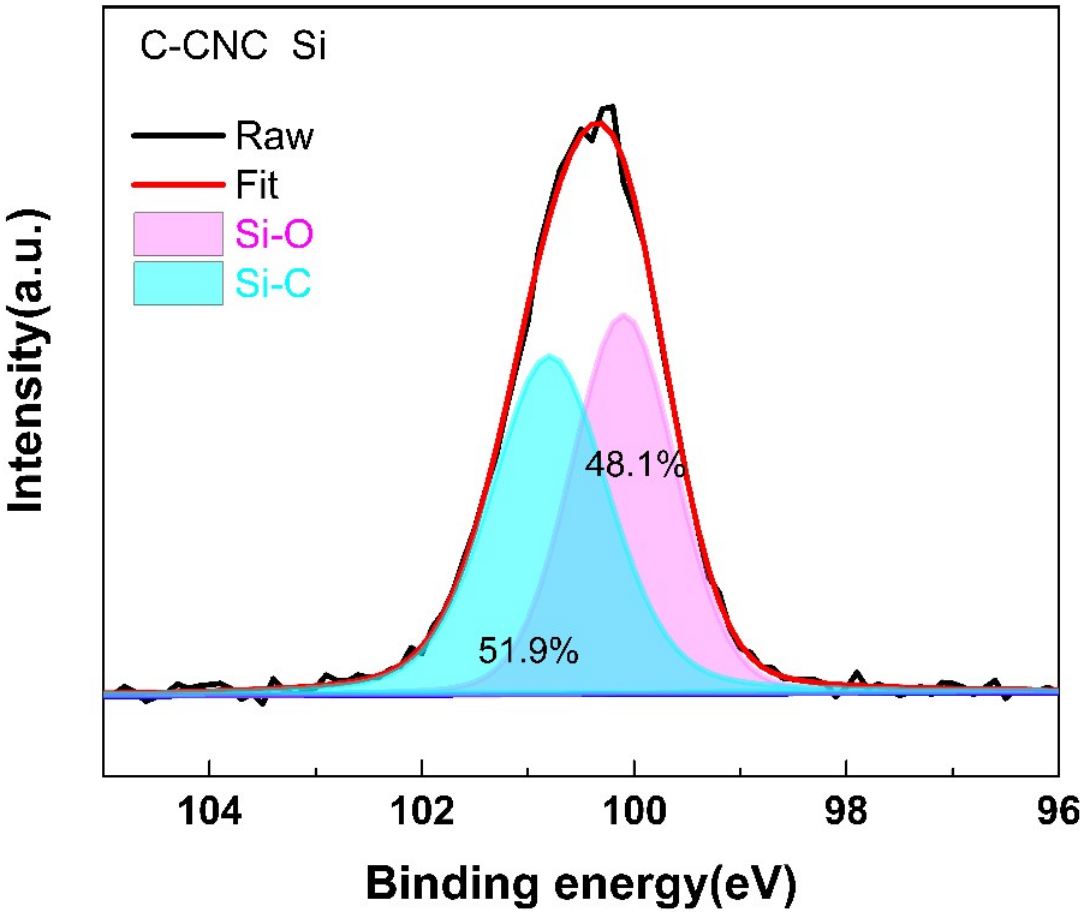

Figure S12 Si 2p curve of C-CNC aerogel

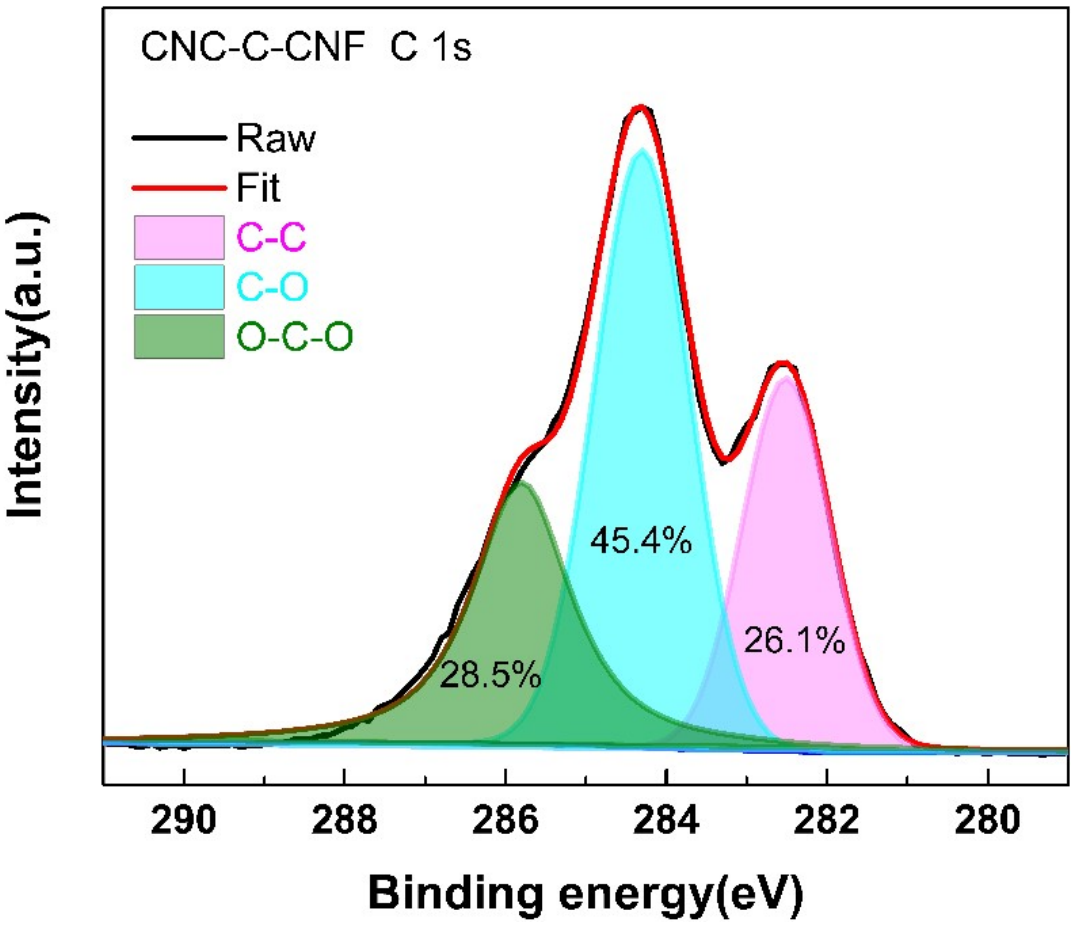

Figure S13 C 1s curve of CNC-C-CNF aerogel (NCA)

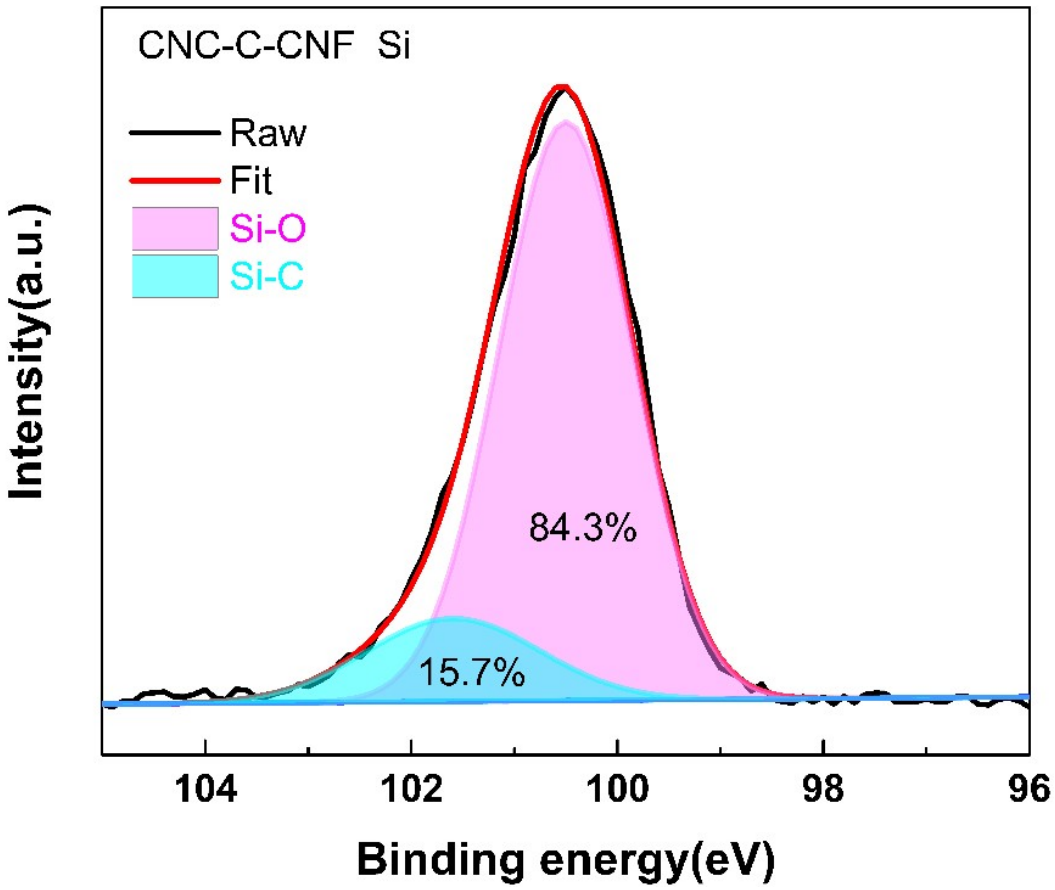

Figure S14 C 1s curve of CNC-C-CNF aerogel (NCA)

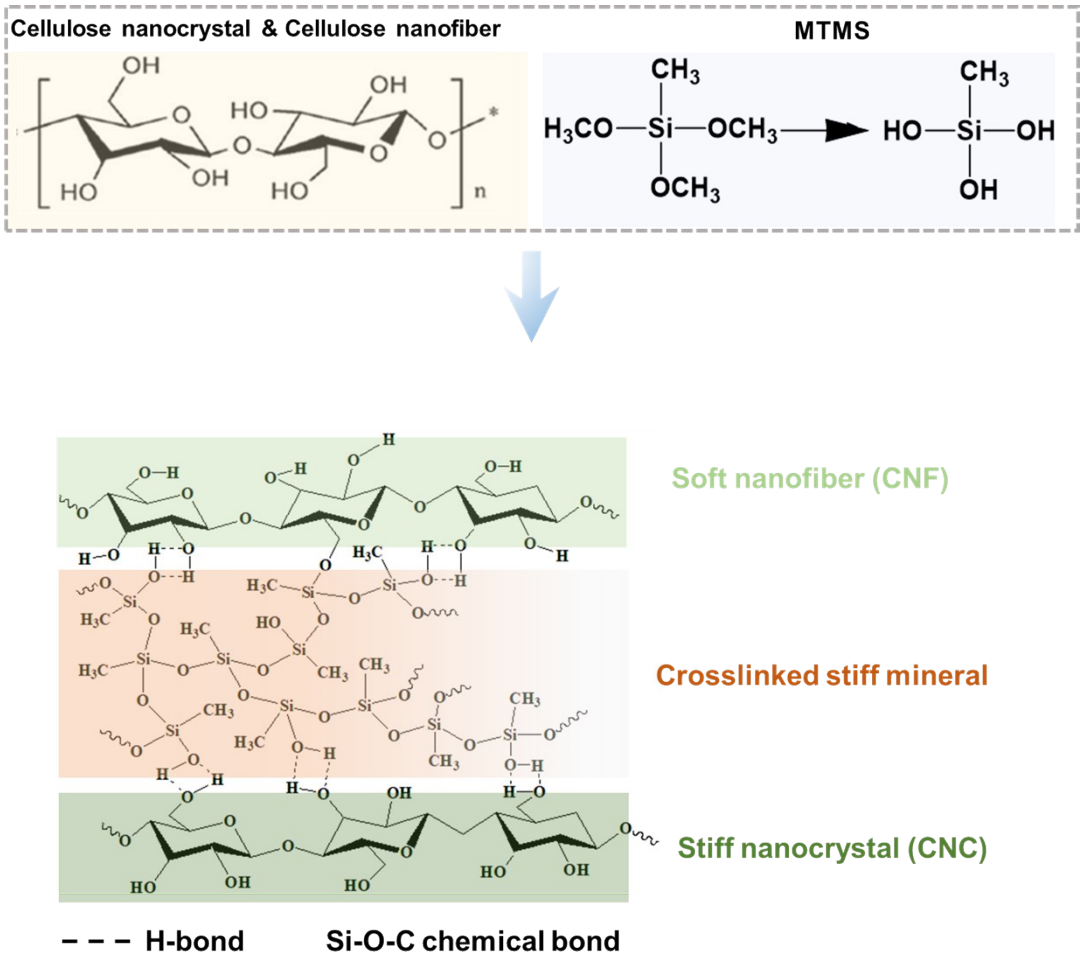

Figure S15 Reaction process and resulting chemical structure of NCA

Figure S16 Optical images of CAN, PE foam and PS foam after heating

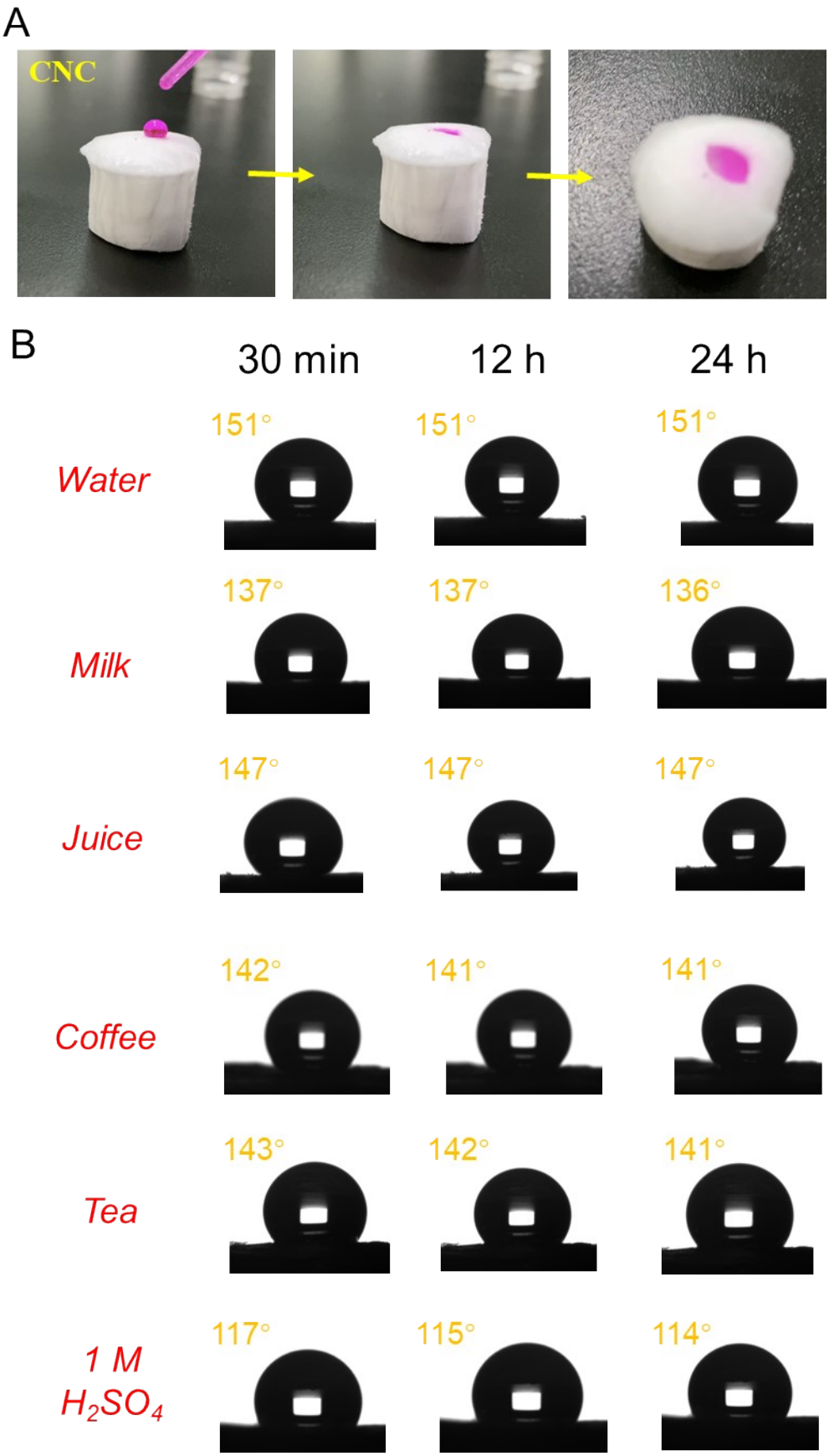

Figure S17 (A) Superhydrophilicity property of pure cellulose nanocrystal aerogel; (B) Contact angle of NCA with different times and solutions

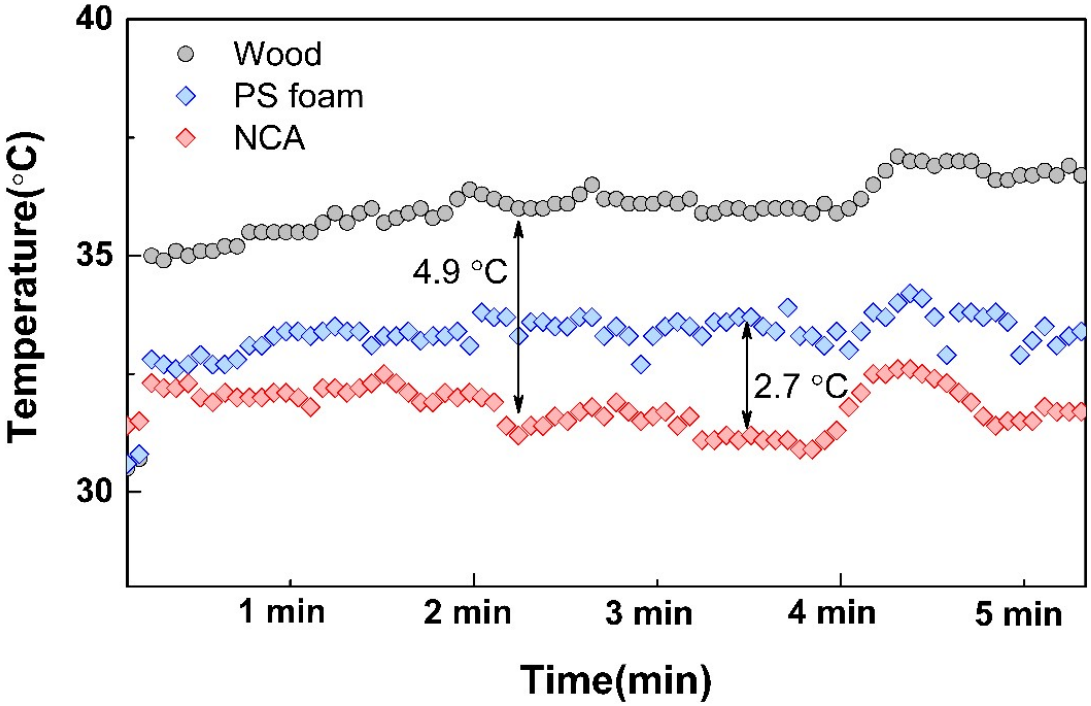

Figure S18 Surface temperature of Wood, PS foam and NCA under 1 sun

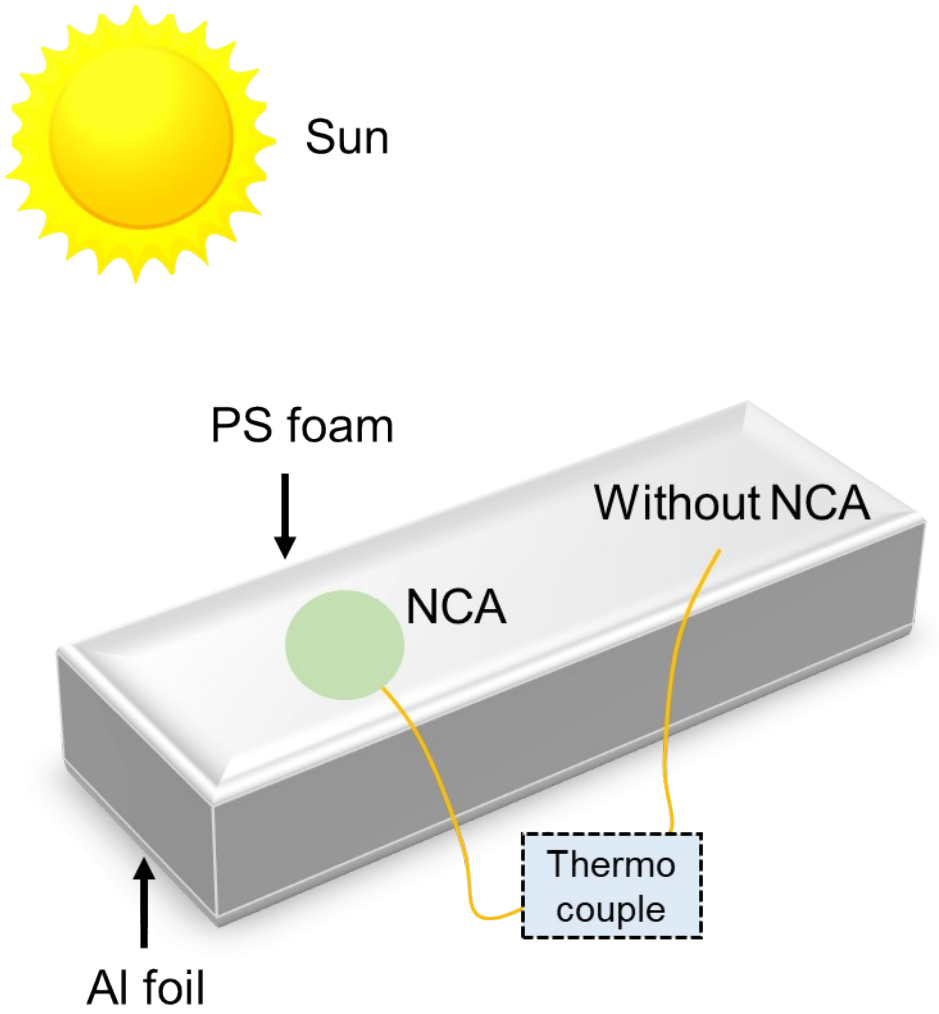

Figure S19 Schematic of testing cooling performance of NCA in Nanjing (China).

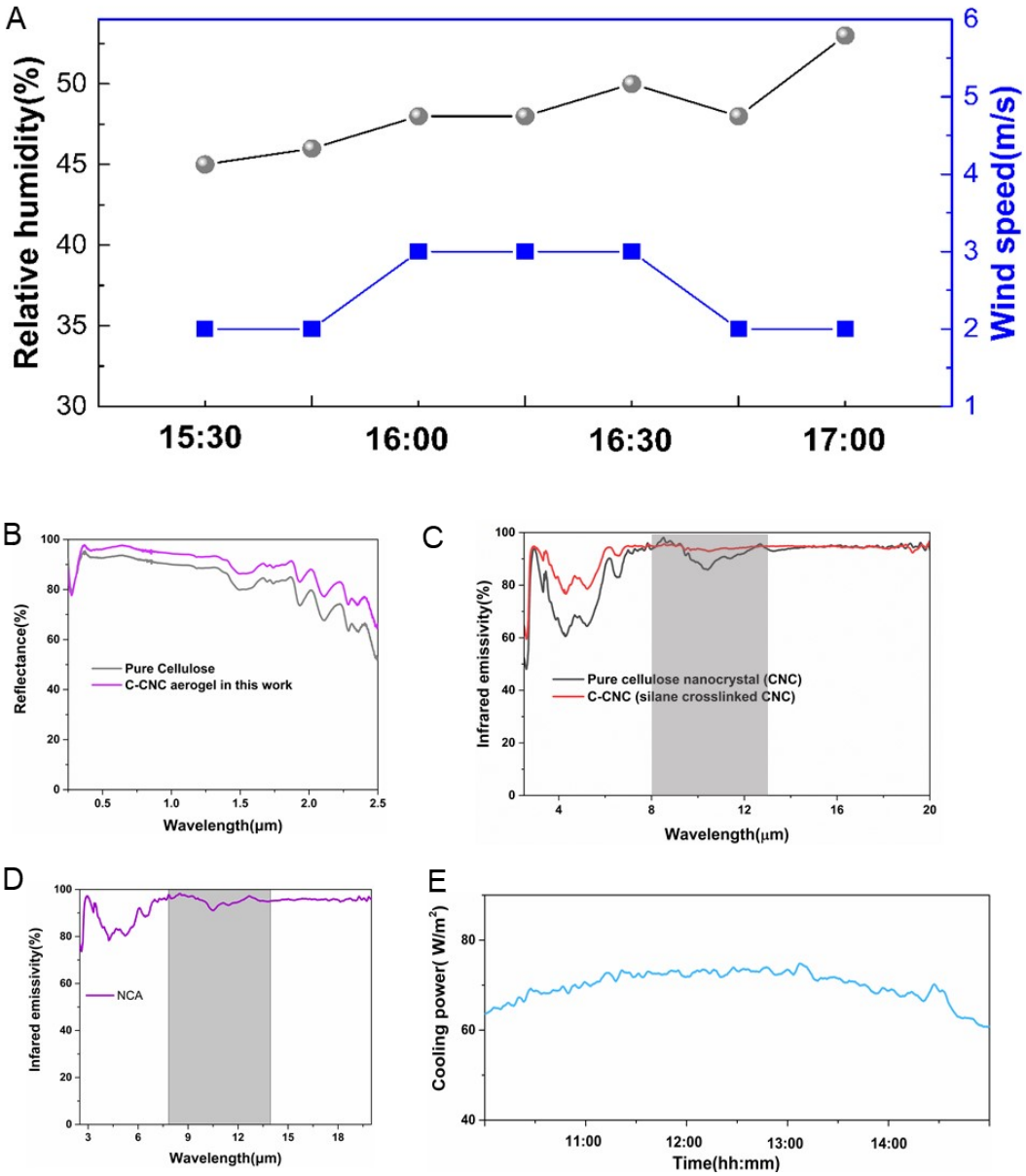

Figure S20 (A) Curves of relative humidity and wind speed during radiative cooling test in Nanjing; (B) Solar reflectance of pure CNC and C-CNC; (C) IR emissivity of pure CNC and C-CNC; (D) IR emissivity of NCA; (E) Cooling power of NCA

Supplementary Note 1 Structure deformation of NCA under a compression state at an oblique angle

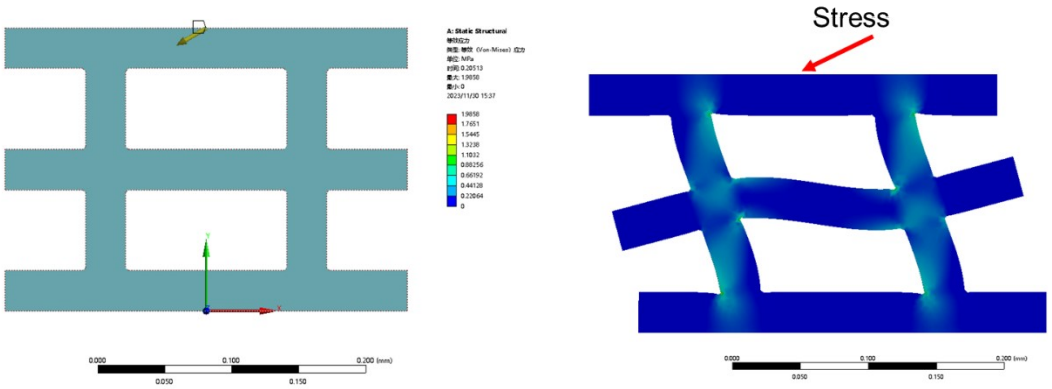

Furtherly, to understand the inner morphology change under a compression state at an oblique angle, the finite element simulation was also conducted. Different from deformation mechanism under traditional compression model, it can be seen that the distorted deformation of floors can be easily observed due to the strong connection with pillars, which can dissipate the energy dramatically. Meanwhile, the pillars shows small shift followed by the direction of stress, which can bear the large amount of force.

Supplementary Note 2 Calculation of solar reflection and infrared emissivity

The solar reflectivity R_{solar} of NCA was calculated as follows:

$$R_{solar}=\frac{\int_{0.3}^{2.5} R(\lambda).\, I_{AM1.5} IAM1.5(\lambda)d\lambda}{\int_{0.3}^{2.5} I_{AM1.5} I(\lambda)d\lambda} \quad (1)$$

The NCA is not transparent, so the infrared emissivity is equal to absorptivity, which = 1- measured reflectivity.

The average thermal emittance $\varepsilon_{8\text{-}13}$ could be calculated as follows:

$$E_{8\text{-}13=}\frac{\int_{8}^{13} \varepsilon(\lambda).\, IBB(\lambda,T)d\lambda}{\int_{8}^{13} IBB(\lambda,T)d\lambda} \quad (2)$$

where λ is the wavelength, $R(\lambda)$ is the surface's spectral reflectance at wavelength λ, $I_{AM1.5}(\lambda)$ is AM 1.5 global solar spectral irradiance, and $\varepsilon(\lambda) = 1\text{-}R(\lambda)$ is the surface's spectral thermal emittance at wavelength λ.

Additionally, $I_{BB}(\lambda, T) = \frac{2hc^2}{\lambda^2} * \frac{1}{e^{hc/\lambda k_B T} - 1}$ (3)

$I_{BB}(\lambda, T)$ is the spectral radiance of a blackbody defined by Planck's law at temperature *T*, where h is Planck's constant, k_B is the Boltzmann constant, *c* is the speed of light in vacuum.

Supplementary Note 3 Finite Element Simulations

The finite element simulation is carried out using commercial code ABAQUS 6.10. The CPS4R, a 4-node bilinear plane stress quadrilateral element is used to mesh both the NCA model. For the purpose of comparison, we keep the thickness of the channel walls in the WC structure model and the curved layers in the WCS structure model roughly the same, while strictly maintaining the same height (21.875 length unit), the same length (35 length unit), and same width (35 length unit) of the entire model. The mathematic description of the curved shape is a sinusoidal function, but it adopts a straight-line shape at the contact region between layers. Then an initial separation (0.5 length unit) between the curved layers is introduced in the WCS structure model for defining the contact between surfaces. Such a contact is modeled by using hard contact as the normal behavior and frictionless resistance as the tangential behavior. Displacement loading is applied as shown in Figure S14. The elastic properties are set as the following - Young's Modulus: 10 GPa, Poisson's ratio: 0.3.

Supplementary Note 4 Cooling energy saving simulation

To evaluate the potential of NCA for energy saving-building, a building energy simulation was put forward by using EnergyPlus version 9.5.0. The building model without ACA consisted of envelopes with baseline properties, including roofs (with an emissivity of 0.9, solar reflectivity of 0.3 and thermal conductivity of 0.16 W m^{-1} K^{-1}) and walls (with an emissivity of 0.9, solar reflectivity of 0.1 and thermal conductivity of 0.6 W m^{-1} K^{-1}) according to our previous studies. For the building model with NCA, an NCA envelope with well thermal-regulation function obtained in this work was placed on surface of the baseline envelope. The indoor temperature was controlled at 25 °C. The cooling energy consumptions of the building models with and without ACA were calculated for different cities in China based on the climate data, which can be found from the EnergyPlus website (https://energyplus.net/weather).

Table S1 Price of NCA (size of 1 m x 1 m)

Product	Market price	Aerogel (100X100X1 cm)	Price (1 m x 1m)
This work (Aerogel Grating)	CNC: 8 $ /g MTMS: 13 $ /100 mL CNF: 1.2 $ /g	CNC: 200 mg MTMS: 15 mL CNF: 400 mg	4.02 $

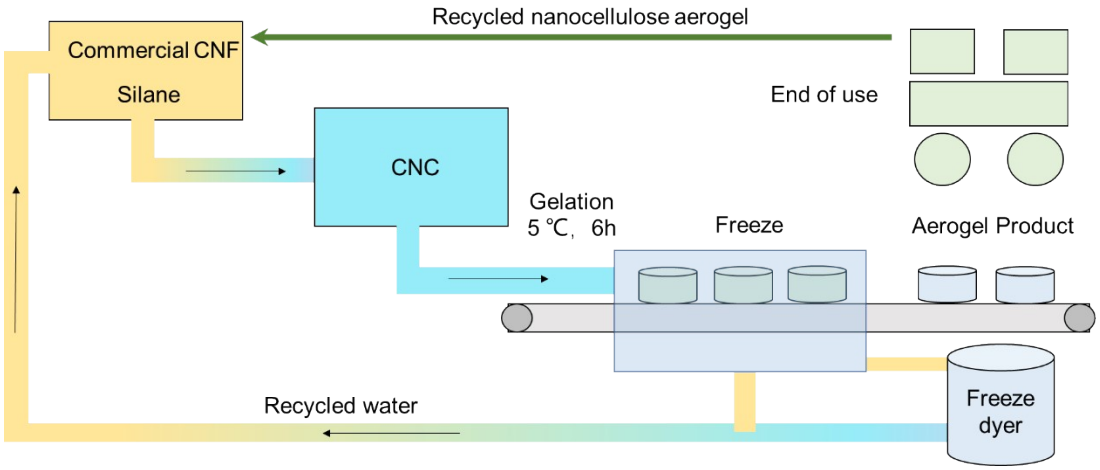

Figure S21 Flow diagram for continuous production and the recycling process of the NCA after its end-of-use.

The fabrication speed of aerogel includes: (1) cutting into species crusher (5 min); (2) redispersing (8 h ultrasonic); (3) stirring (4 h); (4) freeze casting (48 h), and the total time is nearly 60 h. We can produce the aerogel cooler with the maximum scale of 20 x 20 cm by using this method.

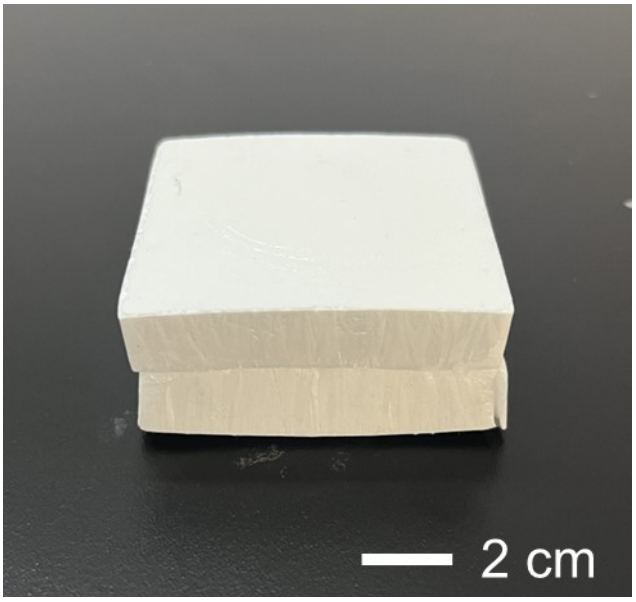

Figure S22 Scalable ability of NCA

Supplementary Note 5

COMSOL stimulation:

The NCA domain was set as a porous medium, where solar reflection and absorption took place on the top surface and pores. The heat transfer in the Aerogel grating could be described as

$$E_{in} = (\rho C_P)_{eff}\frac{\partial T}{\partial t} + PC_P\nabla T + \nabla_q$$

$$q = -k_{eff}\nabla T$$

$$(\rho C_p)_{eff} = \theta_p\rho_p C_{P,P} + (1-\theta_P)\rho C_p$$

$$K_{eff} = \theta_p k_p + (1-\theta_{p)\mathrm{k}}$$

where Ein is the incident heat flux (W m^{-3}), ρ denotes the density of aerogel grating (kg m^{-3}), Cρ is the water capacity at constant pressure (J kg^{-1} K^{-1}), (ρCρ)eff is the effective volumetric heat capacity at constant pressure (J m^{-3} K^{-1}), which is defined by an averaging model to explain aerogel networks, q denotes the conductive heat flux (W m−2), keff is the effective thermal conductivity (W m^{-1} K^{-1}), which is defined by an averaging model to interpret solid matrix and fluid properties. θp and kp is the volume fraction and thermal conductivity of the porous matrix (W m^{-1} K^{-1}).

The boundary conditions were set as constant heat flux of 974 W corresponding to the solar energy input on the surface (consumed 2.6% solar input energy flux (1000 W) as a calculated result). The side walls were set as an open boundary condition, which was explained as free energy exchange with the environment. The mesh elements were performed as a finer grid. Through solving the above equations, the heat transfer process in the NCA system can be fully presented. The thermal conductivity was set as 0.03 W m^{-1} K^{-1}.

Supplementary Note 6 Relationship between pore size and optical/mechanical properties of NCA

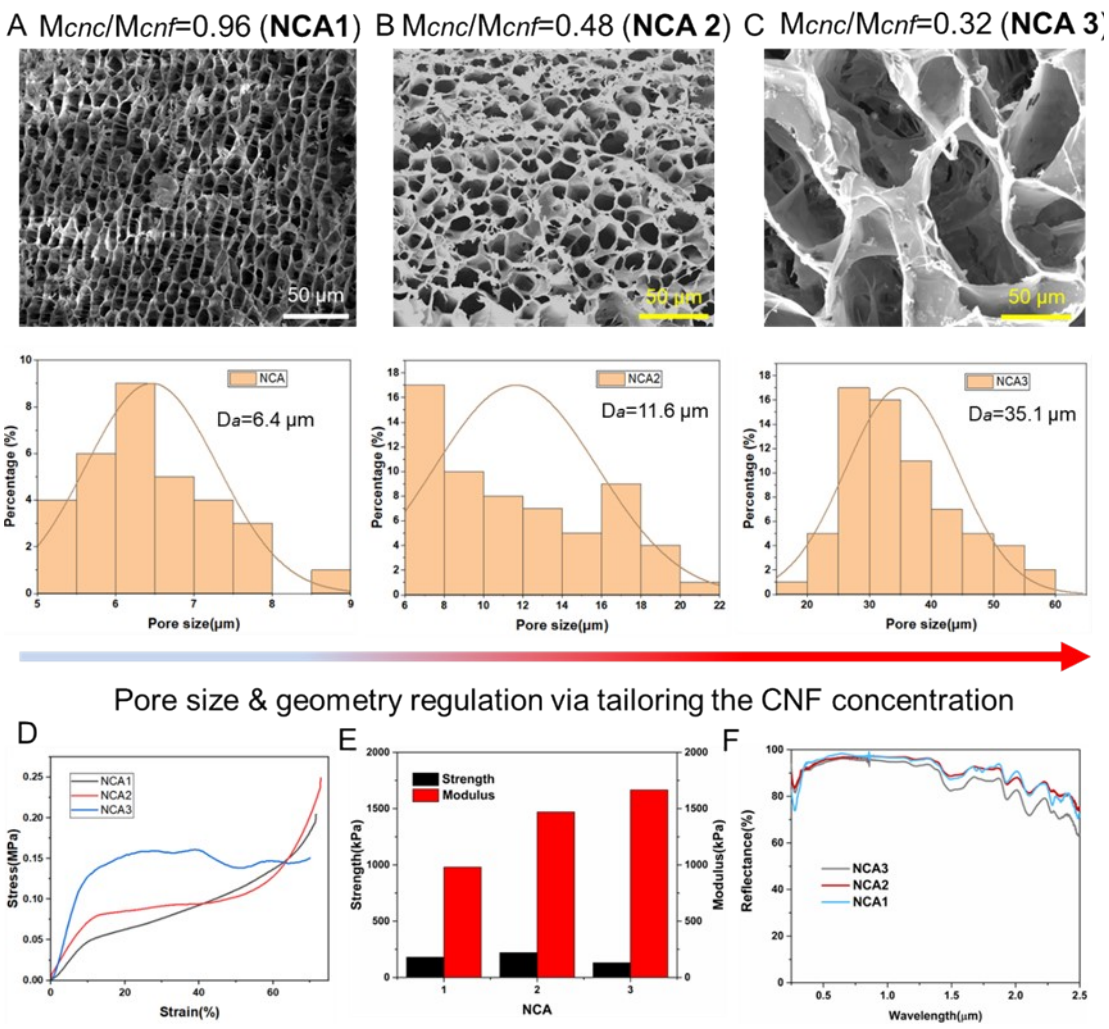

Figure S23 Evaluation of optical and mechanical properties of NCA via tailoring the

pore sizes with changing the CNF concentration.

The pore size and pore geometry can be controllable by this method (by tailoring the CNF concentration). We also tested the optical reflectivity and mechanical properties of NCA with different pore size, as shown in Figure S23. It can be found that with the CNF concentration increased, the pore size showed increase trend, as shown in Figure S23A. After the calculation, the NCA1 showed pore size of 6.4 μm but the NCA3 showed the pore size of 35.1 μm. We also tested the mechanical and optical performance of NCA with different pore sizes, as shown in Figure R4D-F. With the pore size increased from 6.4 to 11.6 μm, the mechanical strength and Young's modulus increased. When the pore size reach up to 35.1 μm, the NCA3 showed poor mechanical performance. Meanwhile, the solar reflectance of NCA showed decreased trend with the pore size increased due to the poor solar scattering ability of big pores in aerogels.

References

1. Cai, C.; Wei, Z.; Huang, Y.; Wang, P.; Song, J.; Deng, L.; Fu, Y., Bioinspired structure-robust cellulose nanocrystal films with enhanced water resistance, photothermal conversion ability, and fluorescence. *Cellulose* **2020,** *27* (17), 10241-10257.